Potential seasonal calibration for palaeoenvironmental reconstruction using skeletal microstructures and strontium measurements from the cold-water coral *Lophelia pertusa*

Vincent Mouchi[1*], Quentin G. Crowley[1], Andrew L. Jackson[2], Frank McDermott[3,4], Xavier Monteys[5], Marc de Rafélis[6,7], José Luis Rueda[8], Franck Lartaud[9,10]

[1]: Department of Geology, School of Natural Sciences, Trinity College Dublin, Museum Building, College Green, Dublin 2, Republic of Ireland

[2]: Department of Zoology, School of Natural Sciences, Trinity College Dublin, Zoology Building, College Green, Dublin 2, Republic of Ireland

[3]: School of Geological Sciences, University College Dublin, Belfield, Dublin 4, Republic of Ireland

[4]: Earth Institute, University College Dublin, Belfield, Dublin 4, Republic of Ireland

[5]: Geological Survey of Ireland, Beggars Bush, Haddington Road, Dublin 4, Republic of Ireland

[6]: Sorbonne Universités, UPMC Univ. Paris 06, UMR 7193, ISTEP, F-75005, Paris, France

[7]: CNRS UMR 7193, ISTEP, F-75005, Paris, France

[8]: Centro Oceanográfico de Málaga, Instituto Español de Oceanografía, Puerto Pesquero s/n, 29620 Málaga, Spain

[9]: CNRS UMR 8222, Laboratoire d'Ecogéochimie des Environnements benthiques, LECOB, Observatoire Océanologique, F-66650 Banyuls-sur-mer, France

[10]: Sorbonne Universités, UPMC Univ Paris 06, UMR 8222, Laboratoire d'Ecogéochimie des Environnements benthiques, Observatoire Océanologique de Banyuls, LECOB, Observatoire océanologique, F-66650, Banyuls-sur-mer, France

[*]: Corresponding author: Vincent Mouchi – Department of Geology, Museum Building, Trinity College Dublin, College Green, Dublin 2, Ireland. E-mail: mouchiy@tcd.ie. Phone: +353 1896 2675.

Abstract

Lophelia pertusa is a colonial cold-water coral species with a wide spatial distribution in recent marine waters. Analyzing the chemistry of its skeleton allows reconstruction of environmental parameters variations. While numerous studies have attempted to interpret such analyses, little information is available on the microstructures of *Lophelia pertusa* and their temporal constraints.

This study introduces newly recognised microstructures in the coral wall following growth along the radial axis. The thicknesses of these 'micro-layers' are correlated with strontium concentrations and can be used to estimate seasonal growth rates of single polyps from the colony. We propose that each of these micro-layers represents a period of one month of mineralization and can locate two decreasing periods in growth rate during a year: one caused by limited food availability during winter months and one in autumn linked to gametogenesis. High-frequency study of strontium concentrations using this interpretation shows a lunar cycle.

We demonstrate that while the micro-layers are present in all *L. pertusa* specimens from four locations in the Atlantic Ocean and the Mediterranean Sea, growth patterns reveal a complex organization that limits their visibility. Strontium fluctuations however appear to be a promising mechanism by which to establish a temporal calibration.

Keywords: Lophelia pertusa, microstructure, growth rate, cold-water corals, strontium

Introduction

Azooxanthellate cold-water corals such as *Lophelia pertusa*, *Madrepora oculata* and *Desmophyllum dianthus* are widely distributed in the marine environment, with the only known exceptions being the Bering Sea and the high Arctic regions (Roberts *et al*., 2009). The depth range of occurrence of these scleractinians is also wide, ranging from 40 meters in Norwegian waters (Trondheimsfjord) to 6,300 meters in the Aleutian Trench. This observation implies that water characteristics (e.g. temperature and salinity) rather than depth are a major factor in their distribution (Keller, 1976). The establishment and development of living colonies in specific areas are favoured by strong currents that generally promote oxygenation, food supply and removal of accumulated sediment particles and waste products (White, 2007; Foubert *et al*., 2008; Davies *et al*., 2009; Mienis *et al*., 2012). *Lophelia pertusa* (Linnaeus, 1758) is a colonial species that generally occurs in deep-sea areas around the world (Davies *et al*., 2008; Roberts *et al*., 2009). As a reef building species, this scleractinian constructs a three-dimensional aragonitic structure that serves as a habitat for a large number of invertebrate and fish species that use it as a sheltered location for feeding, spawning and nursing. Habitats formed by *L. pertusa* colonies generally

55 display an overall increase in biodiversity and productivity compared with adjacent areas where these cold-water
56 corals are absent (Costello *et al*., 2005; Henry and Roberts, 2007; Soffker *et al*., 2011; Biber *et al*., 2014).
57 In terms of modes of growth, scleractinian corals build their skeletons with aragonitic needles from centres of
58 calcification along the theca (Gladfelter, 1982). Unlike tropical corals that display differential density layers that
59 facilitate tomographic imaging (Saenger *et al*., 2009; Cantin *et al*., 2010) cold-water corals do not appear to build
60 such layers. Nevertheless, growth structures defined by opaque and translucent bands in the coral wall as
61 revealed by transmitted light have been described in the skeletons of cold-water corals, including *L. pertusa*
62 (Wainwright, 1964). These bands were originally interpreted as annual patterns (Lazier *et al*., 1999) but it has
63 recently been demonstrated that this is not necessarily the case for either *D. dianthus* (Adkins *et al*., 2004) or *L.*
64 *pertusa* (Gass and Roberts, 2011). As a result, their use in establishing temporal calibrations is in doubt.
65 Biogenic carbonates produced by *L. pertusa* can be used as archives for environmental reconstruction through
66 the use of geochemical proxies for various physico-chemical parameters such as temperature (Smith *et al*.,
67 2000; Case *et al*., 2010), pH (Blamart *et al*., 2007) and water mass circulation (Colin *et al*., 2010; Copard *et al*.,
68 2010; van de Flierdt *et al*., 2010). Productivity has also been investigated for other cold-water coral species (the
69 scleractinian *D. dianthus*: Montagna *et al*., 2006; and for non scleractinian corals, such as bamboo corals:
70 LaVigne *et al*., 2011). One advantage of colonial species for environmental studies is the timeframe over which
71 reconstructions can be achieved, covering several hundred years as a colony grows. The wide distribution of *L.*
72 *pertusa* makes it a coral of choice for this type of study, as a single reconstruction model can be used over a
73 large latitudinal range in the Quaternary fossil record.
74 Although several studies have attempted to use geochemical proxies from the skeletons of *L. pertusa* for
75 environmental reconstructions, geochemical data which appear to follow the skeletal growth by crossing these
76 visible bands have proved to be difficult to interpret (Lutringer *et al*., 2005; Rollion-Bard *et al.*, 2010; Marali *et al*.,
77 2013; Raddatz *et al*., 2013; Robinson *et al.*, 2014). Despite the relatively widespread use of *L. pertusa* in such
78 environmental research, no studies to date have attempted to resolve skeletal microstructures and to correlate
79 these in a systematic way with observed geochemical variations.
80 Meaningful interpretations of high resolution (annual to infra-annual) geochemical fluctuations in biogenic
81 structures require a robust understanding of growth rates and microstructures to ensure a coherent chronological
82 model in relation to the sampling strategy. However, information on growth rates of organisms is exceedingly

difficult to obtain in deep-sea environments where direct long term monitoring is generally not feasible. Previous information on *L. pertusa* growth was determined under laboratory conditions (Orejas *et al*., 2011a; Larsson *et al*., 2013), or from living colonies that had attached to man-made structures, allowing calculation of a mean growth rate (Duncan, 1877). Growth rates for *L. pertusa* colonies inferred using this latter method are highly variable, in the range 3.2 mm a^{-1} (Larcom *et al*., 2014) to 34 mm a^{-1} (Gass and Roberts, 2006) depending on the geographic region and local hydrodynamics. These values however, which correspond to the growth of the whole colony, are primarily driven by the rate of new polyp addition rather than the growth rates of individual polyps (Lartaud *et al*., 2014), which hampers precise temporal calibration of geochemical profiles. Growth rates of corallites (i.e. of the wall and septal thickness) are even less well constrained and it remains unclear how long an individual polyp can live within the colony. Recent mark and recapture techniques developed to study the skeletal growth of individual corallites of *L. pertusa* indicate low growth rates for adult polyps (< 4 mm a^{-1}) but with large variations according to environmental variability (Gulf of Mexico, Mediterranean Sea) (Brooke and Young, 2009; Lartaud *et al*., 2013). Additionally, a strong ontogenic trend is observed in the septal growth rate between newly formed (< 1 year old; 7.5 mm a^{-1}) and old (> 1 year; 1.3 mm a^{-1}) corallites (Lartaud *et al*., 2013). Generally, growth rates of invertebrates are not constant over ontogeny (von Bertalanffy growth model) or even over a single year, due to changes in environmental physicochemical parameters such as temperature as well as food supply (Anderson and Sabado, 1995; Houlbrèque *et al*., 2003; Herrera *et al*., 2012). Variation in growth rates may also result in a temporal modulation of the energy allocated by the organism for its growth (Mortensen, 2001; Orejas *et al*., 2011b). Therefore, growth rates in *L. pertusa* remain difficult to estimate and are poorly constrained.

This study addresses these problems by presenting a novel protocol for documenting microstructures in *L. pertusa*. Using acid etching followed by scanning electron microscope (SEM) imaging this technique is capable of revealing previously unrecognised structural micro-layers from which it is possible to define temporally coherent growth zones. It is thereby possible to estimate individual growth rates and construct a radial temporal calibration across the skeletal wall. To establish this protocol, several tests were carried out on *L. pertusa* specimens from various locations to ensure that the observed response was species-specific and not locality-specific. Specimens were collected from the Whittard Canyon and Porcupine Seabight (Irish waters, north-

eastern Atlantic), the Gulf of Cádiz (Spain, north-eastern Atlantic) and the Lacaze-Duthiers Canyon (France, western Mediterranean Sea) (Fig. 1).

We have studied changes in microstructure patterns, distribution and thickness and performed geochemical analyses of strontium (Sr); a commonly used palaeothermometer proxy) to characterize fluctuations that we consider to have been induced by short-term (infra-annual) variations in environmental conditions, or in a specific metabolic response to those changes.

Figure 1

Material and Methods

During several cruises, living and dead specimens of *L. pertusa* were collected in Irish waters from the Whittard Canyon (cruises CE-12006 and CE-13008) and the Porcupine Seabight (cruise CE-13001), in the Gulf of Cadiz (cruises Indemares-Chica 0610, 0211 and 0412) and from the Lacaze-Duthiers canyon in the Mediterranean Sea (UPMC-Fondation TOTAL cruises 2010, 2011 and 2013, R/V Minibex from the COMEX Company) as shown in Table 1 and Figure 1. Dead specimens were typically 5 to 15 cm long at most, usually representing several polyps as the colony grew. Specimens that were living at the time of collection were cut from the colony at the end of branches to extract pieces c. 4 to 5 cm long.

Table 1

Skeletal areas for microstructural analyses were preferentially selected where the distance between polyps was at its greatest. Following collection, all specimens were cleaned using hydrogen peroxide (H_2O_2, 3.4% at 60˚C or 5% at room temperature) and rinsed in deionised water in an ultrasonic bath several times. To screen for possible diagenetic alteration of the aragonitic needles and to characterize any recrystallization in calcite, XRD analysis was performed in the School of Natural Sciences, Trinity College Dublin (Ireland) and cathodoluminescence observation was performed at the Institut des Sciences de la Terre de Paris (ISTeP,

Université Pierre et Marie Curie, Paris, France). Samples showing recrystallization were removed from the set of specimens to be analyzed.

Three specimens were processed using serial cutting (slides approximately 0.5 mm thick) using an Isomet Low-Speed Saw following mounting in EpoFix resin. All other specimens (21 from all locations) were mounted on regular thick (0.5 to 1 mm) sections. These were cut along the longitudinal axis following the maximum growth extension, as opposed to the radial axis where mineralization is slower (Fig. 2). Using a protocol modified from Nothdurft and Webb (2007), sections were then polished and etched on both sides with 2% formic acid for 50 seconds. Observations of the theca were performed at the Centre for Microscopy and Analysis at Trinity College Dublin using a Tescan Mira XMU SEM in secondary electron mode at 15 kV following gold coating.

Figure 2

Exceptionally well developed and continuous microstructures were studied in details and thicknesses of micro-layers revealed by the etching protocol were measured from the centres of calcification (COC) following the radial growth from a specimen collected in the Whittard Canyon (WhC-1). Sr concentrations were measured on the same section in the Trinity College Dublin geochemistry facility using a Thermo Scientific iCAP Q ICP-MS, coupled with an Analyte Excite laser ablation system performing 20 by 180 µm line rasters at 35 $\mu m.s^{-1}$ and a 5 Hz repetition rate. NIST 612 was used as a calibration standard. The error on Sr measurements was less than 2.1% (2 SE). Raw Sr concentrations were smoothed by moving average and this was subtracted from the raw data. A Fast Fourier Transform (FFT) was performed on the resulting residuals to isolate the cyclicities present in the high-frequency fluctuations in Sr content.

Results

SEM observations

Our etching-imaging protocol has revealed micro-layers along the radial growth direction of the wall in some sections for each of the 24 samples from all locations (Fig. 3). Importantly, no microstructures are visible along the longitudinal axis. Micro-layers observed along the radial growth direction are generally parallel to each other,

but in some areas the micro-layers present a curved pattern toward the outer part of the skeleton within a restricted area (150 to 200 µm in length; Fig. 3-b). In these parts a bulge is visible on all micro-layers from the inner-most part of the skeleton (near the COC) to the surface of specimen on the outer-most layer. There is no compensation visible on the edges of the bulge to reduce the irregularity and thus the thicknesses of the micro-layers overall remain unchanged. Some aragonite fibres are interrupted by the change of micro-layer direction, but these fibres are observed to occur in the same general orientation from one layer to the next.

Figure 3

Only one section of a sample from Whittard Canyon (specimen WhC-1) shows micro-layers across the entire wall. In order to reduce the possibility of missing these structures, serial cuts of an entire corallite specimen (each section about 0.5 mm thick prior to polishing and etching) were performed on 3 samples. Despite this attention to detail, we failed to produce a section with at least one face exhibiting all the sets of micro-layers as was the case for specimen WhC-1. In all of the specimens treated with this technique, the outermost sections did not display any layers in the microstructure. In the sections from the innermost part of the calyx, some micro-layers were partially visible, but none presented continuous structures as observed in WhC-1.

For most coral sections examined as part of this study, micro-layers are not revealed in all areas of the theca but they are always present in some parts of the wall (Fig. 4). Areas of dense, compact aragonite (not in the form of fibres) are commonly visible and can be found either in continuity with the micro-layers or between two series of micro-layers along the axial growth direction.

Figure 4

Opaque bands in most specimens seem to prevent the development of layered mineralization (Fig. 5). Micro-layers are visible only in optically translucent bands. The specimen WhC-1 does not exhibit any opaque and translucent bands in reflected light. This is likely to be significant in terms of formation of well-developed microstructures described here.

Figure 5

Discontinuous micro-layers are also visible in some sections in areas filled with aragonite fibres (Fig. 6). In these cases, the continuity of the visible micro-layer can be observed only for a few dozen microns and it is never possible in this case to quantify them.

Figure 6

Micro-layer thickness

The micro-layers range in thickness from approximately 20 to 100 µm (Table 2) and are organized in successive groups of similar thicknesses. WhC-1 contains 23 micro-layers across the wall. Successive thicknesses measured from the COC to the outer edge of the wall show fluctuations with four observed cycles (Fig. 7).

Table 2

Figure 7

Strontium concentrations

Sr measurements across the wall of WhC-1 show strong fluctuations (from 6041 ppm ± 126 ppm to 12067 ppm ± 252 ppm, mean 8703 ppm). Smoothed data (Fig. 7) reveal a negative trend, with lower values at the outer edge compared to the inner part of the skeleton. A comparison of layer thickness with Sr concentrations along the radial growth direction reveals that these two parameters fluctuate in phase, implying a distinct physio-chemical response presumably linked to some change in environmental conditions and / or growth rate (Fig. 7). It is apparent that higher values of Sr in the coral skeleton tend to be coincident with the occurrence of thick micro-layers.

Depending on the thickness of the micro-layers, each increment has between 3 and 14 measurements of Sr. By splitting the dataset equally as thin (3-8 points per micro-layer) and thick (9-14 points per micro-layer)

increments, the mean number of analysis are 5.47 points per thin micro-layer and 11.75 points per thick micro-layer respectively.

A highly significant group of frequencies in the residuals from the smoothed data (Fig. 8) is revealed by FFT, centred at the value 6.25 points per cycle. Cycles corresponding to this frequency can be observed both in thick layers (two cycles per layer) and thin layers (one cycle per layer). A second frequency is also revealed at 12.5 points per cycle. No other frequencies are significant.

Figure 8

Discussion

Micro-layer occurrence

The micro-layers described here are thinner and more numerous than the optically visible opaque and translucent bands described in *L. pertusa* by Wainwright (1964). For specimen WhC-1 there is a conspicuous lack of opaque bands. The fact that micro-layers are not visible on all sections implies that *L. pertusa* skeletons display a more complex organization than a common linear growth model. This could be due to the growth of patches of aragonite fibres (related to different growth phases) in a three-dimensional sense, that do not follow the radial growth direction in a simple manner. This is particularly clear on sections where only some growth micro-layers can be found between areas where fibres are not visible (e.g. Fig. 6). This implies that the orientation and position of the section are important factors in obtaining visibly extensive micro-layers.

Micro-scale layers have previously been observed in solitary coral species (Sorauf and Jell, 1977; Lazier *et al*., 1999; Cheng *et al*., 2000; Marali *et al*., 2013). Growth structures of less than 10 μm in thickness were observed in *D. dianthus* (Lazier *et al*., 1999) and intrinsic timekeeping mechanisms (i.e. “biological clocks”) were proposed as the cause. *Caryophyllia cyathus* and *Stenocyathus vermiformis* were also investigated (Marali *et al*., 2013) but the authors observed features that impeded interpretation, as some layers were merging or pinching out, preventing a chronological tracking. The micron-scale space between these layers is revealed by etching. It is therefore possible this space is filled with a more porous, organic-rich carbonate structure that would deteriorate easily in the presence of acid.

Temporal Calibration of the micro-layers

The cyclic pattern of layer thickness may be caused by variations in growth rate over the life of the polyp. Sclerochronology uses layers in growth structures to establish temporal calibrations as they are assumed to have been built by the organism over similar timescales regardless of their thickness (Marchitto *et al*., 2000; Carré *et al*., 2005; Schöne and Gillikin, 2013). Accepting this hypothesis it is possible to consider here that narrow layers reflect periods with low growth rates compared to thicker layers. High growth rates generally correspond to periods of favourable conditions during which the organism can allocate more energy to growth, as has been established in different cnidarians (Mortensen, 2001; Houlbrèque *et al*., 2003; Orejas *et al*., 2011b) and other invertebrate groups (Jolivet, 2009; Lartaud *et al*., 2010). In corals, such cycles composed of a period of high growth rate followed by one of lower growth rate can be assumed to reflect diurnal patterns for shallow water species (Wells, 1963) or annual patterns for cold-water species (Cheng *et al*., 2000) with even longer periods possible as induced by local environmental influence such as the North Atlantic Oscillation (NAO) as observed in bivalves (Schöne *et al*., 2003).

There are several different possible causes for observed growth rate changes observed in our *Lophelia pertusa* specimens. Due to the thickness of some micro-layers (reaching 100 μm), it is unlikely that such structures can represent a single day of mineralization along the radial axis, particularly considering the colony (mainly longitudinal) growth rates recorded in the literature (3.2 to 34 $mm.a^{-1}$). A NAO case of annual banding can be proposed to explain a multi-annual fluctuation, however the colony growth rates are not compatible with this timeframe. Considering a radial growth of 20 to 100 μm per year while the colony grows at a rate of several mm per year, the polyps would generate brittle theca that would be prone to being broken in an area with strong water currents such as their natural habitat. A third possible cause for the observed microstructure banding implies a monthly characteristic of micro-layers based on the lunar cycle. Such a correlation is more consistent with the growth rates measured in *Lophelia pertusa*. Moreover, the cycles observed by the high-frequency fluctuations of Sr incorporation can be used to confirm the influence of the monthly moon revolutions on growth rates and formation of these micro-layers. Both cyclicities recorded (6.25 and 12.5 points per cycle) are close to the mean number of Sr measurements per layer (i.e. 5.47 and 11.75 points per layer, for thin and thick micro-layers respectively), and this must be taken into consideration when evaluating any periodicity in cyclicity. The

cycles corresponding to high growth rates (one cycle in thick micro-layers) and the 12.5 point cycle are compatible with a lunar influence. This pattern would be the equivalent of a lunar month considering the monthly pattern of micro-layer occurrence proposed here. The observed 6.25 point cycle, corresponding to exactly half the time of the cycle described above, can be related to a fortnightly influence. These cycles are only visible in thick micro-layers (i.e. two cycles per layer; Fig. 8). In thinner layers, due to changes in the measured number of points per layer, the fluctuations should be interpreted carefully. With layers measuring only half the thickness of the larger ones of similar temporal value, the observed cycle is most probably double the apparent one, which is the monthly fluctuation proposed above. In other words, due to differences in growth rates between layers, the 6.25 point cycle in thin layers is equivalent of the 12.5 point cycle observed in thicker layers. Such monthly and fortnightly lunar cycles (28 and 14 days, respectively) were previously observed on Mg/Ca measurements in coastal oyster shells from mark-and-recapture experiments (Mouchi *et al*., 2013). Time-related growth patterns have also been observed in deep-sea mussels and linked both to tidal influence (i.e. lunar cycle) on near-bottom currents and to biological clocks (Schöne and Giere, 2005; Schöne, 2008; Nedoncelle *et al*., 2013). As no long-term monitoring of benthic hydrodynamics is available in the sampled locations, neither phenomenon can be ruled out as an explanation for recording tidal influence in the growth increments. Recently, van Haren *et al.* (2014) however have recorded substantial (1.5-2˚C) daily temperature fluctuations at 900 m in the North Atlantic and attributed this to bottom-intensified currents reflecting surface waters conditions. This illustrates that an indirect tidal effect is capable of causing significant and periodic temperature changes in deep benthic water environments. Moreover, Ingels *et al.* (2011) demonstrated that the Porcupine Seabight is subjected to a tidal input of organic matter from the Gollum Channels system. Such tidal currents however have not been described in the Whittard Canyon but turbidity currents have been recorded (Ingels *et al.,* 2011).

Low-frequency change in growth rates

Based on the proposed micro-layer lunar monthly periodicity, the main cycles observed in increment counting, concomitant with those from the Sr signal (Fig. 7), do not correspond to an annual scale. This is contrary to the "classic" model found in calcifying species (Klein *et al.*, 1996; Kirby, 2000; Saenger *et al*., 2009; Cantin *et al*., 2010; Butler *et al.*, 2013; Schöne and Gillikin, 2013; Bougeois *et al.*, 2014). In contrast to the situation in shallow environments, where high temperatures in summer are known to increase growth rates of some invertebrates

(Malone and Dodd, 1967; Schöne *et al*., 2006; Hiebenthal *et al*., 2013), most deep-sea environments are not subjected to the necessary seasonal thermal contrasts to explain this intra-annual variation in growth rates, with the possible exception of spatially restricted areas under the influence of bottom-intensified currents. Cold-water corals may have higher growth rates when food availability increases (Naumann *et al*., 2011) as is the case for other suspension feeders (Houlbrèque *et al*., 2003; Herrera *et al*., 2012). However, Larsson *et al*. (2013) showed that *L. pertusa* can maintain a high growth rate during extended periods of starvation with higher values than observed from previous studies (Orejas *et al*., 2011a; Form and Riebesell, 2012). The diet of *L. pertusa* however is still unclear; azooxanthellate corals were first thought to be detrital feeders only, but Porter (1976) proposed that coral species with larger polyps and long tentacles such as *L. pertusa* were adapted to capture zooplankton. *In situ* observations have provided evidence for some carnivorous behaviour of the species, with occasional consumption of zooplankton and copepods (Freiwald, 2002). In addition to this, Kiriakoulakis *et al*. (2005) have showed that the $\delta^{15}N$ of *L. pertusa* confirmed an occasional carnivorous diet. Due to these uncertainties, diet alone cannot give unequivocal information on whether high growth rates areas occur in summer or winter months. Detrital materials should be present in larger amounts during the winter season, as more weathering occurs on land supplying more material to rivers and eventually to the oceanic waters. On the other hand, primary production in the photic zone is at a maximum during summer, inducing a more significant planktonic vertical flux to the deep benthos (Sigman and Hain, 2012). These uncertainties coupled with a poorly constrained time lag between increased nutrient flux in surface waters and their transport to deep benthic environments also inhibit an understanding of the timing of growth cycles in *L. pertusa.*

In terms of their reproductive biology, it is noteworthy that both *L. pertusa* and *M. oculata* seem to be seasonal broadcasters, with gametogenesis occurring over a seasonally limited time period estimated from August to October in the Porcupine area (Waller and Tyler, 2005). Considering that gametogenesis is a costly mechanism in terms of energy, a decrease in somatic and skeleton growth is expected. Using the seasonality of the reproductive clock of *L. pertusa* observed by Waller and Tyler (2005) and considering that each micro-layer has been synthesized in 28 days, the start of the first micro-layer in the last decrease in growth rate on the transect reported on Figure 7 has been assigned with having been formed on the 1st of August. Using this as a starting point, the rest of the skeleton was assigned months accordingly (Fig. 9). Regarding this interpretation, the August month from the previous year is also occurring during a slow growth period. The other main slow growth periods

329 on the transect correspond to assigned winter months, and may be caused by a decrease in food availability.
330 Importantly, a minor amplitude during the first year could be explained by development of the initial part of the
331 skeleton. It is significant that faster growth rates have been observed in colonies that were fed nauplii under
332 laboratory conditions (Orejas *et al*., 2011a; Larsson *et al*., 2013). Using geographically close populations of
333 Mediterranean *L. pertusa* cultured in aquaria, Orejas *et al*. (2011a) recorded faster growth rate when feeding
334 corals with *Artemia salina* 5 times per week, whereas Lartaud *et al*. (2013) recorded lower growth rates when
335 feeding 3 times per week. These observations are compatible with our interpretation that at least some of the
336 changes in micro-layer thickness, and hence growth rates, are linked to seasonal availability of nutrients.
337
338 Figure 9
339
340 Previous studies performed on solitary corals were not able to characterize timeframes between successive
341 layers and growth rate changes (Lazier *et al*., 1999; Marali *et al*., 2013). Based on mean calculations of absolute
342 dating with U-series techniques on multiple parts of the same specimens, it was however suggested that opaque
343 and translucent bands in *D. dianthus* were formed at a rhythm of 0.3 to 3 per annum (Cheng *et al*., 2000). This
344 implies that micro-scale layers are built at a much higher frequency. However, due to the complexity of the micro-
345 increments in *D. dianthus*, it is difficult to create an inventory of the number of layers in a band, even when
346 considering that bands and layers are both formed in cyclicities, which for *L. pertusa* is not certain.
347 Regarding microstructures along the longitudinal axis of *L. pertusa*, it seems unlikely that they can provide an
348 effective temporal calibration along this direction. This is an important point, as some studies (Cohen *et al*., 2006;
349 López Correa *et al*., 2010) have performed geochemical analyses along a longitudinal axis in an attempt to
350 describe temporally constrained palaeoenvironmental perturbations. In contrast, micro-layers along the radial
351 axis described here and observed on one specimen present a promising tool to establish a seasonal framework
352 within which to interpret geochemical transects along the radial axis. In the case of specimen WhC-1 described
353 above, this would allow reconstruction of a two year record of environmental fluctuations for this specimen.
354 Longer periods could be studied by analyzing successive corallites from the same colony, each with a transect
355 following the layers in the microstructure.
356

Potential misuse of strontium as an environmental proxy

A negative trend in elemental ratios along the growth direction in shells has previously been observed (Mg/Ca, Sr/Ca…) and in numerous taxa from shallow water environments (mussel: Rosenberg and Hughes, 1991; clam: Strasser *et al*., 2008; oyster: Higuera-Ruiz and Elorza, 2009). The processes involved in these ontogenic trends are still unknown. However, positive trends have also been observed in bivalves (Stecher *et al*., 1996; Carre *et al*., 2006; Mouchi *et al*., 2013). Moreover, several studies focussing on the same species and techniques reported positive and negative trends for bivalves (Higuera-Ruiz and Elorza, 2009; Mouchi *et al*., 2013). In deep-sea environments, an ontogenic trend can also be environmental and be caused by a long-term evolution of temperature, for instance. Thus, with respect to the incorporation of Sr, it is not ideal to interpret this trend either as an environmental or as a physiological influence.

In the *L. pertusa* specimen studied here (WhC-1), fluctuations in Sr concentrations are strongly in phase with variations in micro-layers thickness (Fig. 7). If the temporal calibration in Figure 9 is correct, Sr concentrations represent low values during winter months and during gametogenesis, and high values in other periods, showing two cycles in a year and thus refuting a seasonal cycle for Sr variations.

Cyclical fluctuations may be primarily structural in origin in that higher Sr concentrations have also previously been observed in inorganic carbonates (speleothems) when the growth rates increase (Huang and Fairchild, 2001). This observation was also reported in deep-sea (Weber, 1973) and tropical corals (Kuffner *et al*., 2012; Grove *et al*., 2013). However, most studies use Sr/Ca ratios as a proxy for temperature in tropical shallow-water corals (Beck *et al*., 1992; de Villiers *et al*., 1994; Alibert and McCulloch, 1997; Cardinal *et al*., 2001; Chen *et al*., 2013) and seasonal fluctuations have also been investigated for *L. pertusa* (Cohen *et al*., 2006). It has been demonstrated though that Sr incorporation is mainly dependant on calcification rate from studies with shallow water corals (Reynaud *et al*., 2004) and with inorganic aragonite growth experiments (Gaetani and Cohen, 2006). This explanation would indicate that the main process for Sr uptake in coral skeletons is growth rate over temperature. According to the interpretations in the present study, Sr/Ca fluctuations could be incorrectly interpreted as a seasonal pattern, whereas in fact two cycles of Sr incorporation represent a single year of mineralization in Irish waters where the gametogenesis/spawning calendar is as described by Waller and Tyler (2005). If two consecutive cycles (one “environmental” and one “metabolic”) present the same Sr amplitude (as it is the case here), then using this pattern as a temporal calibration to study longer-term (multi-annual) variations

will not be accurate. Future studies should therefore try to discriminate whether Sr fluctuations reflect an annual or a semi-annual pattern in specific study locations in order to correctly interpret geochemical data as a proxy for palaeoenvironmental reconstruction.

In view of the kinetics potentially involved in elemental incorporation into the crystal lattice, it seems invalid to invoke a uniquely temperature dependency of the Sr incorporation in cold-water corals without a proper temporal calibration, as it is the case with shallow-water corals presenting annual density bands. It remains unclear for cold-water corals to what extent growth rate is influenced by the environment as opposed to metabolic processes.

Conclusions

This paper highlights the absolute necessity of microstructure characterisation in any study of geochemistry on biominerals other than bulk assays. Micro-layers have now been observed within the translucent layers of the wall of *L. pertusa* that can be used for intra-annual temporal calibration and analysis of growth rates of polyps. However, the characteristic chaotic pattern in the microstructure of opaque layers prevents formation of micro-layers. Furthermore, non-linear growth phases induce even more complexity and present a challenge to resolve these layers on a single surface.

If a means to study the orientation of growth phases prior to sectioning were to be developed, it would permit the definition of a direction of cutting to reveal the growth micro-layers and thus allow more temporally continuous high-resolution geochemical studies on the wall of *L. pertusa*. Microanalytical geochemical and isotopic studies of *L. pertusa* which are not supported by careful micro-textural characterisations of samples carry the risk of sampling from temporally disparate areas with the consequence of misinterpretation of apparently “seasonal” signals.

We describe a possible interpretation of Sr fluctuations as a means to estimate growth rate that can be used for temporal calibration where two consecutive cycles of Sr are induced by both environmental parameters fluctuation and gametogenesis during a single year. Future work could focus on an elemental mapping in the theca and study the fluctuations in 2-dimensions to characterize temporality on both growth axes.

Acknowledgements

The work presented in this paper was made possible by the ENS PhD programme. The Earth and Natural Sciences Doctoral Studies Programme is funded under the Programme for Research in Third-Level Institutions Cycle-5 and co-funded under the European Regional Development Fund.

Operation of the TCD ICP-MS was supported by FP7-PEOPLE-2011-CIG #293712.

This research was carried out under the Sea Change strategy with the support of the Marine Institute and the Marine Research Sub-program of the National Development Plan 2007-2013. The authors also wish to thank the captains and crews of the *Celtic Voyager* and *Celtic Explorer* along with the CE-12006 and CE-13001 chief scientists Louise Allcock and Glenn Nolan.

Sampling of *L. pertusa* colonies from the Gulf of Cádiz was supported by the INDEMARES/CHICA Project, EC contract INDEMARES-LIFE+ (07/NAT/E/000732) and FEDER funding assigned to equipment of R/V Cornide de Saavedra (FICTS-2010-01) and to construction of R/V Ramón Margalef (FICTS-2011-03-01).

Sampling of *L. pertusa* colonies from the Lacaze-Duthiers canyon was supported by the chair 'Extreme environment, biodiversity and global change' (Foundations TOTAL and UPMC, coordination: N. Le Bris), using the R/V Minibex (COMEX).

References

Adkins JF, Henderson GM, Wang S-L, *et al*. 2004. Growth rates of the deep-sea scleractinia *Desmophyllum cristagalli* and *Enallopsammia rostrata*. *Earth and Planetary Science Letters* **227**: 481-490.

Alibert C, McCulloch M. 1997. Strontium/Calcium ratios in modern *Porites* corals from the Great Barrier Reef as a proxy for sea surface temperature: Calibration of the thermometer and monitoring of ENSO. *Paleoceanography* **12**: 345-363.

Anderson TW, Sabado BD. 1995. Correspondence between food availability and growth of a planktivorous temperate reef fish. *Journal of Experimental Marine Biology and Ecology* **189**: 65-76.

438 Beck JW, Edwards RL, Ito E, *et al*. 1992. Sea-surface temperature from coral skeletal
439 strontium/calcium ratios. *Science* **257**: 644-647.
440 Biber MF, Duineveld GCA, Lavaleye MSS, *et al*. 2014. Investigating the association of fish
441 abundance and biomass with cold water corals in the deep Northeast Atlantic Ocean using a
442 generalized linear modelling approach. *Deep-Sea Research II* **99**: 134-145.
443 Blamart D, Rollion-Bard C, Meibom A, *et al*. 2007. Correlation of boron isotopic
444 composition with ultrastructure in the deep-sea coral *Lophelia pertusa*: Implications for
445 biomineralization and paleo-pH. *Geochemistry Geophysics Geosystems* **8**: Q12001, doi:
446 10.1029/2007GC001686.
447 Bougeois L, de Rafélis M, Reichart G-J, *et al.* 2014. A high resolution study of trace
448 elements and stable isotopes in oyster shells to estimate Central Asian Middle Eocene
449 seasonality. *Chemical Geology* **363**: 200-212.
450 Butler PG, Wanamaker AD Jr, Scourse, JD, *et al*. 2013. Variability of marine climate on the
451 North Icelandic Shelf in a 1357-year proxy archive based on growth increments in the bivalve
452 *Arctica islandica*. *Palaeogeography Palaeoclimatology Palaeoecology* **373**: 141-151.
453 Brooke S, Young CM. 2009. *In situ* measurements of survival and growth of *Lophelia*
454 *pertusa* in the northern Gulf of Mexico. *Marine Ecology Progress Series* **397**: 153-161.
455 Cantin NE, Cohen AL, Karnauskas KB, *et al*. 2010. Ocean warming slows coral growth in
456 the Central Red Sea. *Science* **329**: 322-325.
457 Cardinal D, Hamelin B, Bard E, *et al*. 2001. Sr/Ca, U/Ca and $\delta^{18}O$ records in recent massive
458 corals from Bermuda: relationships with sea surface temperature. *Chemical Geology* **176**:
459 213-233.
460 Carré M, Bentaleb I, Blamart D, *et al*. 2005. Stable isotopes and sclerochronology of the
461 bivalve *Mesodesma donacium*: Potential application to Peruvian paleoceanographic
462 reconstructions. *Palaeogeography Palaeoclimatology Palaeoecology* **228**: 4-25.

463 Carré M, Bentaleb I, Bruguier O, *et al*. 2006. Calcification rate influence on trace element
464 concentrations in aragonitic bivalve shells: evidences and mechanisms. *Geochimica et*
465 *Cosmochimica Acta* **70**: 4906-4920.
466 Case DH, Robonson LF, Auro ME, *et al*. 2010. Environmental and biological controls on Mg
467 and Li in deep-sea scleractinian corals. *Earth and Planetary Science Letters* **300**: 215-225.
468 Chen T, Yu K, Chen T. 2013. Sr/Ca-sea surface temperature calibration in the coral *Porites*
469 *lutea* from subtropical northern South China Sea. *Palaeogeography Palaeoclimatology*
470 *Palaeoecology* **392**: 98-104.
471 Cheng H, Adkins J, Edwards RL, *et al*. 2000. U-Th dating of deep-sea corals. *Geochimica et*
472 *Cosmochimica Acta* **64**: 2401-2416.
473 Cohen AL, Gaetani GA, Lundälv T, *et al*. 2006. Compositional variability in a cold-water
474 scleractinian, *Lophelia pertusa*: new insights into "vital effects". *Geochemistry Geophysics*
475 *Geosystems* **7**: doi: 10.1029/2006GC001354.
476 Colin C, Frank N, Copard K, *et al*. 2010. Neodymium isotopic composition of deep-sea
477 corals from the NE Atlantic: implications for past hydrological changes during the Holocene.
478 *Quaternary Science Review* **29**: 2509-2517.
479 Copard K, Colin C, Douville E, *et al*. 2010. Nd isotopes in deep-sea corals in the North-
480 eastern Atlantic. *Quaternary Science Review* **29**: 2499-2508.
481 Costello MJ, McCrea M, Freiwald A, *et al*. 2005. Role of cold-water *Lophelia pertusa* coral
482 reefs as fish habitat in the NE Atlantic. In *Cold-water Corals and Ecosystems*, Freiwald A,
483 Roberts JM (eds). Springer: Berlin Heidelberg; 771–805.
484 Davies AJ, Wisshak M, Orr JC, *et al*. 2008. Predicting suitable habitat for the cold-water
485 coral *Lophelia pertusa* (Scleractinia). *Deep-Sea Research I* **55**: 1048-1062.

Davies AJ, Duineveld GCA, Lavaleye MSS, *et al*. 2009. Downwelling and deep-water bottom currents as food supply mechanisms to the cold-water coral *Lophelia pertusa* (Scleractinia) at the Mingulay Reef complex. *Limnology and Oceanography* **54**: 620-629.

de Villiers S, Shen GT, Nelson BK. 1994. The Sr/Ca-temperature relationship in coralline aragonite: Influence of variability in $(Sr/Ca)_{seawater}$ and skeletal growth parameters. *Geochimica et Cosmochimica Acta* **58**: 197-208.

Duncan PM. 1877. On the rapidity of growth and variability of some Madreporaria on an Atlantic Cable, with remarks upon the rate of accumulation of foraminiferal deposits. *Proceedings of the Royal Society of London* **26**: 133-137.

Form AU, Riebesell U. 2012. Acclimation to ocean acidification during long-term CO_2 exposure in the cold-water coral *Lophelia pertusa*. *Global Change Biology* **18**: 843-853.

Foubert A, Depreiter D, Beck T, *et al*. 2008. Carbonate mounds in a mud volcano province off northwest Morocco: key to processes and controls. *Marine Geology* **248**: 74-96.

Freiwald A. 2002. Reef-forming cold-water corals. In *Ocean Margin Systems*, Wefer G, Billett D, Hebbeln D, *et al*. (eds). Springer: Berlin Heidelberg; 365-385.

Gaetani GA, Cohen AL. 2006. Element partitioning during precipitation of aragonite from seawater: A framework for understanding paleoproxies. *Geochimica et Cosmochimica Acta* **70**: 4617-4634.

Gass SE, Roberts JM. 2006. The occurrence of the cold water coral *Lophelia pertusa* (Scleractinia) on oil and gas platforms in the North Sea: colony growth, recruitment and environmental control on distribution. *Marine Pollution Bulletin* **52**: 549-559.

Gass SE, Roberts JM. 2011. Growth and branching patterns of *Lophelia pertusa* (Scleractinia) from the North Sea. *Journal of Marine Biological Association of the United Kingdom* **91**: 831-835.

510 Gladfelter EH. 1982. Skeletal development in *Acropora cervicornis*: I. Patterns of calcium
511 carbonate accretion in the axial corallite. *Coral Reefs* **1**: 45-51.
512 Grove CA, Brummer G-JA, Kasper S, *et al*. 2013. Confounding effects of coral growth and
513 high SST variability on skeletal Sr/Ca: Implications for coral paleothermometry.
514 *Geochemistry Geophysics Geosystems* **14**: doi: 10.1002/ggge.20095.
515 Henry LA, Roberts JM. 2007. Biodiversity and ecological composition of macrobenthos on
516 cold-water coral mounds and adjacent off-mound habitat in the bathyal Porcupine Seabight,
517 NE Atlantic. *Deep-Sea Research I* **54**: 654-672.
518 Herrera I, Yebra L, Hernández-Léon S. 2012. Effect of temperature and food concentration
519 on the relationship between growth and AARS activity in *Paracartia grani* nauplii. *Journal*
520 *of Experimental Marine Biology and Ecology* **416-417**: 101-109.
521 Hiebenthal C, Philipp EER, Eisenhauer A, *et al*. 2013. Effects of seawater pCO_2 and
522 temperature on shell growth, shell stability, condition and cellular stress of Western Baltic
523 Sea *Mytilus edulis* (L.) and *Arctica islandica* (L.). *Marine Biology* **160**: 2073-2087.
524 Higuera-Ruiz R, Elorza J. 2009. Biometric, microstructural, and high-resolution trace
525 element studies in *C. gigas* of Cantabria (Bay of Biscay, Spain): anthropogenic and seasonal
526 influences. *Estuarine, Coastal and Shelf Science* **82**: 201-213.
527 Houlbrèque F, Tambutté E, Ferrier-Pagès C. 2003. Effect of zooplankton availability on the
528 rates of photosynthesis, and tissue and skeletal growth in the scleractinian coral *Stylophora*
529 *pistillata*. *Journal of Experimental Marine Biology and Ecology* **296**: 145-166.
530 Huang Y, Fairchild IJ. 2001. Partitioning of Sr^{2+} and Mg^{2+} into calcite under karst-analogue
531 experimental conditions. *Geochimica et Cosmochimica Acta* **65**: 47-62.
532 Ingels J, Tchesunov AV, Vanreusel A. 2011. Meiofauna in the Gollum Channels and the
533 Whittard Canyon, Celtic Margin – How local environmental conditions shape nematode
534 structure and function. *Plos One* **6** (5): e20094. doi: 10.1371/journal.pone.0020094.

Jolivet A. 2009. Compréhension des mécanismes de Biominéralisation : quantification spatialisée des fractions minérale et organique et influence de facteurs environnementaux. Ph.D. thesis, Universite de Bretagne Occidentale, 254 p.

Keller NB. 1976. The deep-sea madreporarian corals of the genus *Fungiacyathus* from the Kurile-Kamchatka, Aleutian Trenches and other regions of the world oceans. *Trudy Institut Okeanologii* **99**: 31-44 (in Russian).

Kirby MX. 2000. Paleoecological differences between Tertiary and Quaternary *Crassostrea* oysters, as revealed by stable isotope sclerochronology. *Palaios* **15**: 132-141.

Kiriakoulakis K, Fisher E, Wolff GA, *et al*. 2005. Lipids and nitrogen isotopes of two deep-water corals from the North-East Atlantic: initial results and implications for their nutrition. In *Cold-water Corals and Ecosystems*, Freiwald A, Roberts JM (eds). Springer: Berlin Heidelberg; 715-729.

Klein RT, Lohmann KC, Thayer CW. 1996. Bivalve skeletons record sea-surface temperature and $\delta^{18}O$ via Mg/Ca and $^{18}O/^{16}O$ ratios. *Geology* **24**: 415-418.

Kuffner IB, Jokiel PL, Rodgers KS, *et al*. 2012. An apparent “vital effect” of calcification rate on the Sr/Ca temperature proxy in the reef of coral *Montipora capitata*. *Geochemistry Geophysics Geosystems* **13**: doi: 10.1029/2012GC004128.

Larcom EA, McKean DL, Brooks JM, *et al*. 2014. Growth rates, densities, and distributions of *Lophelia pertusa* on artificial structures in the Gulf of Mexico. *Deep Sea Research I* **85**: 101-109.

Larsson AI, Lundälv T, van Oevelen D. 2013. Skeletal growth, respiration rate and fatty acid composition in the cold-water coral *Lophelia pertusa* under varying food conditions. *Marine Ecology Progress Series* **483**: 169-184.

Lartaud F, de Rafélis M, Ropert M, *et al*. 2010. Mn labelling of living oysters: artificial and natural cathodoluminescence analyses as a tool for age and growth rate determination of *C. gigas* (Thunberg, 1793) shells. *Aquaculture* **300**: 206-217.

Lartaud F, Pareige S, de Rafélis M, *et al*. 2013. A new approach for assessing cold-water coral growth in situ using fluorescent calcein staining. *Aquatic Living Resources* **26**: 187-196.

Lartaud F, Pareige S, de Rafélis M, *et al*. 2014. Temporal changes in the growth of two Mediterranean cold-water coral species, in situ and in aquaria. *Deep Sea Research II* **99**: 64-70.

LaVigne M, Hill TM, Spero HJ, *et al*. 2011. Bamboo coral Ba/Ca: Calibration of a new deep ocean refractory nutrient proxy. *Earth and Planetary Science Letters* **312**: 506-515.

Lazier AV, Smith JE, Risk MJ, *et al*. 1999. The skeletal structure of *Desmophyllum cristagalli*: the use of deep-water corals in sclerochronology. *Lethaia* **32**: 119-130.

López Correa M, Montagna P, Vendrell-Simón B, *et al*. 2010. Stable isotopes ($\delta^{18}O$ and $\delta^{13}C$), trace and minor element compositions of Recent scleractinians and Last Glacial bivalves at the Santa Maria di Leuca deep-water coral province, Ionian Sea. *Deep-sea Research II* **57**: 471-486.

Lutringer A, Blamart D, Frank N, *et al*. 2005. Paleotemperatures from deep-sea corals: scale effects. In *Cold-water Corals and Ecosystems*, Freiwald A, Roberts JM (eds). Springer: Berlin Heidelberg; 1081-1096.

Malone PG, Dodd JR. 1967. Temperature and salinity effects on calcification rate in *Mytilus edulis* and its paleoecological implications. *Limnology and Oceanography* **12**: 432-436.

Marali S, Wisshak M, López Correa M, *et al*. 2013. Skeletal microstructure and stable isotope signature of three bathyal solitary cold-water corals from the Azores. *Palaeogeography Palaeoclimatology Palaeoecology* **373**: 25-38.

582 Marchitto TM Jr, Jones GA, Goodfriend GA, *et al*. 2000. Precise temporal correlation of
583 Holocene mollusc shells using sclerochronology. *Quaternary Research* **53**: 236-246.
584 Mienis F, De Stigter HC, De Haas H, *et al*. 2012. Hydrodynamic conditions in a cold-water
585 coral mound area on the Renard Ridge, southern Gulf of Cadiz. *Journal of Marine Systems*
586 **96-97**: 61-71.
587 Montagna P, McCulloch M, Taviani M, *et al*. 2006. Phosphorus in cold-water corals as a
588 proxy for seawater nutrient chemistry. *Science* **312**: 1788-1791.
589 Mortensen PB. 2001. Aquarium observations on the deep-water coral *Lophelia pertusa* (L.,
590 1958) (scleractinia) and selected associated invertebrates. *Ophelia* **54**: 83-104.
591 Mouchi V, de Rafélis M, Lartaud F, *et al*. 2013. Chemical labelling of oyster shells used for
592 time-calibrated high-resolution Mg/Ca ratios: A tool for estimation of past seasonal
593 temperature variations. *Palaeogeography Palaeoclimatology Palaeoecology* **373**: 66-74.
594 Naumann MS, Orejas C, Wild C, *et al*. 2011. First evidence for zooplankton feeding
595 sustaining key physiological processes in a scleractinian cold-water coral. *Journal of*
596 *Experimental Biology* **214**: 3570-3576.
597 Nedoncelle K, Lartaud F, de Rafélis M, *et al*. 2013. A new method for high-resolution
598 bivalve growth rate studies in hydrothermal environments. *Marine Biology* **160**: 1427-1439.
599 Nothdurft LD, Webb G. 2007. Microstructure of common reef-building coral genera
600 *Acropora*, *Pocillopora*, *Goniastrea*, and *Porites*: constrains on spatial resolution in
601 geochemical sampling. *Facies* **53**: 1-26.
602 Orejas C, Ferrier-Pagès C, Reynaud S, *et al*. 2011a. Long-term growth rates of four
603 Mediterranean cold-water coral species maintained in aquaria. *Marine Ecology Progress*
604 *Series* **429**: 57-65.

605 Orejas C, Ferrier-Pagès C, Reynaud S, *et al*. 2011b. Experimental comparison of skeletal
606 growth rates in the cold-water coral *Madrepora oculata* Linnaeus, 1758 and three tropical
607 sceractinian corals. *Journal of Experimental Biology and Ecology* **405**: 1-5.
608 Porter JW. 1976. Autotrophy, heterotrophy, and resource partitioning in Caribbean reef-
609 building corals. *American Naturalist* **110**: 731-742.
610 Raddatz J, Liebetrau V, Ruggeberg A, *et al*. 2013. Stable Sr-isotope, Sr/Ca, Mg/Ca, Li/Ca
611 and Mg/Li ratios in the scleractinian cold-water coral *Lophelia pertusa*. *Chemical Geology*
612 **352**: 143-152.
613 Reynaud S, Ferrier-Pagès, Boisson F, *et al.* 2004. Effect of light and temperature on
614 calcification and strontium uptake in the scleractinian coral *Acropora verweyi*. *Marine*
615 *Ecology Progress Series* **279**: 105-112.
616 Roberts JM, Wheeler AJ, Freiwald A, *et al*. 2009. Cold Water Corals: the Biology and
617 Geology of Deep-Sea Coral Habitats. Cambridge University Press: Cambridge.
618 Robinson LF, Adkins JF, Frank, N, *et al.* 2014. The geochemistry of deep-sea coral
619 skeletons : A review of vital effects and applications for palaeoceanography. *Deep-Sea*
620 *Research II* **99**: 184-198.
621 Rollion-Bard C, Blamart D, Cuif J-P, *et al*. 2010. *In situ* measurements of oxygen isotopic
622 composition in deep-sea coral, *Lophelia pertusa*: Re-examination of the current geochemical
623 models of biomineralization. *Geochimica et Cosmochimica Acta* **74**: 1338-1349.
624 Rosenberg GD, Hughes WW. 1991. A metabolic model for the determination of shell
625 composition in the bivalve mollusc, *Mytilus edulis*. *Lethaia* **24**: 83-96.
626 Saenger C, Cohen AL, Oppo DW, *et al*. 2009. Surface-temperature trends and variability in
627 the low-latitude North Atlantic since 1552. *Nature Geoscience* **2**: 492-495.
628 Schöne BR. 2008. The curse of physiology-challenges and opportunities in the interpretation
629 of geochemical data from mollusc shells. *Geo-Marine Letters* **28**: 269-285.

630 Schöne BR, Oschmann W, Rössler J, *et al*. 2003. North Atlantic Oscillation dynamics
631 recorded in shells of a long-lived bivalve mollusc. *Geology* **31**: 1037-1040.
632 Schöne BR, Giere O. 2005. Growth increments and stable isotope variation in shells of the
633 deep-sea hydrothermal vent bivalve mollusc *Bathymodiolus brevior* from the North Fiji
634 Basin, Pacific Ocean. *Deep-sea Research I* **52**: 1896-1910.
635 Schöne BR, Rodland DL, Fiebig J, *et al*. 2006. Reliability of multitaxon, multiproxy
636 reconstructions of environmental conditions from accretionary biogenic skeletons. *Journal of*
637 *Geology* **114**: 267-285.
638 Schöne BR, Gillikin DP. 2013. Unraveling environmental histories from skeletal diaries –
639 Advances in sclerochronology. *Palaeogeography Palaeoclimatology Palaeoecology* **373**: 1-
640 5.
641 Sigman DM, Hain MP. 2012. The biological productivity of the ocean. *Nature Education*
642 *Knowledge* **3**: (10) 21.
643 Smith JE, Risk MJ, Schwarcz HP, *et al*. 2000. Paleotemperatures from deep-sea corals:
644 overcoming "vital effects". *Palaios* **15**: 25-32.
645 Soffker M, Sloman KA, Hall-Spencer JM. 2011. In situ observations of fish associated with
646 coral reefs off Ireland. *Deep-Sea Research I* **58**: 818-825.
647 Sorauf JE, Jell JS. 1977. Structure and incremental growth in the ahermatypic coral
648 *Desmophyllum cristagalli* from the North Atlantic. *Palaeontology* **20**: 1-19.
649 Stecher HA, Krantz DE, Lord III CJ, *et al*. 1996. Profiles of strontium and barium in
650 *Mercenaria mercenaria* and *Spisula solidissima* shells. *Geochimica et Cosmochimica Acta*
651 **60**: 3445-3456.
652 Strasser CA, Mullineaux LS, Walther BD. 2008. Growth rate and age effects on *Mya arenia*
653 shell chemistry: implications for biogeochemical studies. *Journal of Experimental Marine*
654 *Biology and Ecology* **355**: 153-163.

655 Van de Flierdt T, Robinson LF, Adkins JF. 2010. Deep-sea coral aragonite as a recorder for
656 the neodymium isotopic composition of seawater. *Geochimica et Cosmochimica Acta* **74**:
657 6014-6032.
658 Van Haren H, Mienis F, Duineveld GCA, *et al*. 2014. High-resolution temperature
659 observations of a trapped nonlinear diurnal tide influencing cold-water corals on the
660 Logachev mounds. *Progress in Oceanography* **125**: 16-25.
661 Wainwright SA. 1964. Studies of the mineral phase of coral skeleton. *Experimental Cell*
662 *Research* **34**: 213-230.
663 Waller RG, Tyler PA. 2005. The reproductive biology of two deep-water, reef-building
664 scleractinians from the NE Atlantic Ocean. *Coral Reefs* **24**: 514-522.
665 Weber JN. 1973. Incorporation of strontium into reef coral skeletal carbonate. *Geochimica et*
666 *Cosmochimica Acta* **37**: 2173-2190.
667 Wells JW. 1963. Coral growth and geochronometry. *Nature* **197**: 948-950.
668 White M. 2007. Benthic dynamics at the carbonate mound regions at the Porcupine Sea Bight
669 continental margin. *International Journal of Earth Sciences* **96**: 1-9.
670

671

Location	Coordinates	Water depth range (m)	Alive or dead polyps
Whittard Canyon (WhC)	48°28'N, 10°45'W	650-800	Alive and Dead
Porcupine Seabight (PoS)	49°49'N, 13°57'W	340 to 365	Dead
Gulf of Cadiz (GoC)	36°41'N, 7°08'W	350 to 800	Dead
Lacaze-Duthiers Canyon (LDC)	42°15'N, 3°25'E	500 to 520	Alive

672

673 Table 1: Locations of sampled specimens.

674

675

Micro-layers	Thickness (μm)
1	95
2	65
3	80
4	85
5	95
6	65
7	40
8	35
9	40
10	95
11	55
12	45
13	35
14	20
15	30
16	30
17	45
18	105
19	100
20	55
21	45
22	40
23	50

676

677 Table 2: Micro-layers thicknesses in specimen WhC-1.

678 Figure captions

679

680 Figure 1: Map of sampling locations. PoS: Porcupine Seabight. WhC: Whittard Canyon. GoC: Gulf of Cadiz.
681 LDC: Lacaze-Duthiers Canyon.

682

683 Figure 2: WhC-1 *Lophelia pertusa* specimen. Orientation of cutting is marked with a dashed line.

684

685 Figure 3: Micro-layers imaged in the theca wall of *L. pertusa*. a: In specimen WhC-1. The longitudinal growth
686 direction is towards the bottom right and radial growth towards the upper right. The scale bar is 200 µm. b: Detail
687 of the micro-layers on the area delimited by the white square in Figure 3a. Longitudinal growth direction is
688 towards right. Radial growth direction is upward. Scale bar is 100 µm. c: Specimen LDC-5. The longitudinal
689 growth direction is towards the upper right and radial growth towards the bottom right. The scale bar is 100 µm.
690 d: Interpretation of c. e: Specimen GoC-2. The longitudinal growth direction is towards the right and radial growth
691 towards the bottom. The scale bar is 50 µm. f: Interpretation of e. g: Specimen PoS-1. The longitudinal growth
692 direction is towards the left and radial growth towards upward. The scale bar is 50 µm. h: Interpretation of g.
693 COC: centres of calcification.

694

695 Figure 4: Absence of micro-layers in the middle of the wall near the corallite (on the left) in specimen WhC-1.
696 Micro-layers are visible on the right hand side when moving away from the corallite (but are not visible in this
697 view). The thick black curve highlights the COC. The scale bar is 200 µm long.

698

699 Figure 5: Opaque and translucent bands (centre) in relation to traces of micro-layers under SEM (left) in
700 specimen WhC-3c and interpretation (right). On the right-hand side, white areas represent opaque bands and
701 grey areas represent translucent bands, and black dashed lines represent micro-layers visible from the SEM
702 figure. Longitudinal growth is towards the right; radial growth is towards the top. The scale bar is 100 µm long.

703

704 Figure 6: a: Micro-layers with no continuity visible in specimen GoC-2/2d. b: Interpretation of a. Black lines
705 represent visible micro-layers and fine grey lines represent aragonite fibres. Note that micro-layers are visible

only where aragonite fibres can be seen. Longitudinal growth direction is towards the right; radial growth direction is towards the top. The scale bar is 100 µm long.

Figure 7: Strontium concentrations (in grey) across the wall of specimen WhC-1 in relation to micro-layer thickness (in black). The micro-layer thickness values are positioned at the center of each of these increments starting with the first complete (the space between the COC and the first increment was ignored). Sr concentrations have been smoothed using a moving average. Error bars for Sr concentrations are less than the line width. The arrow indicates the location of the COC.

Figure 8: Residuals of strontium measurements on WhC-1 (in black) in relation to micro-layers occurrence (vertical grey dashed lines).

Figure 9: Micro-layers thickness and interpreted monthly calibration (on top) across the wall of WhC-1. The micro-layer starting at 1160 µm was used as the starting point of the proposed temporal frame. In this interpretation, 1 micro-layer is formed in 28 days.

Table 1: Locations of sampled specimens.

Table 2: Micro-layers thicknesses in specimen WhC-1.

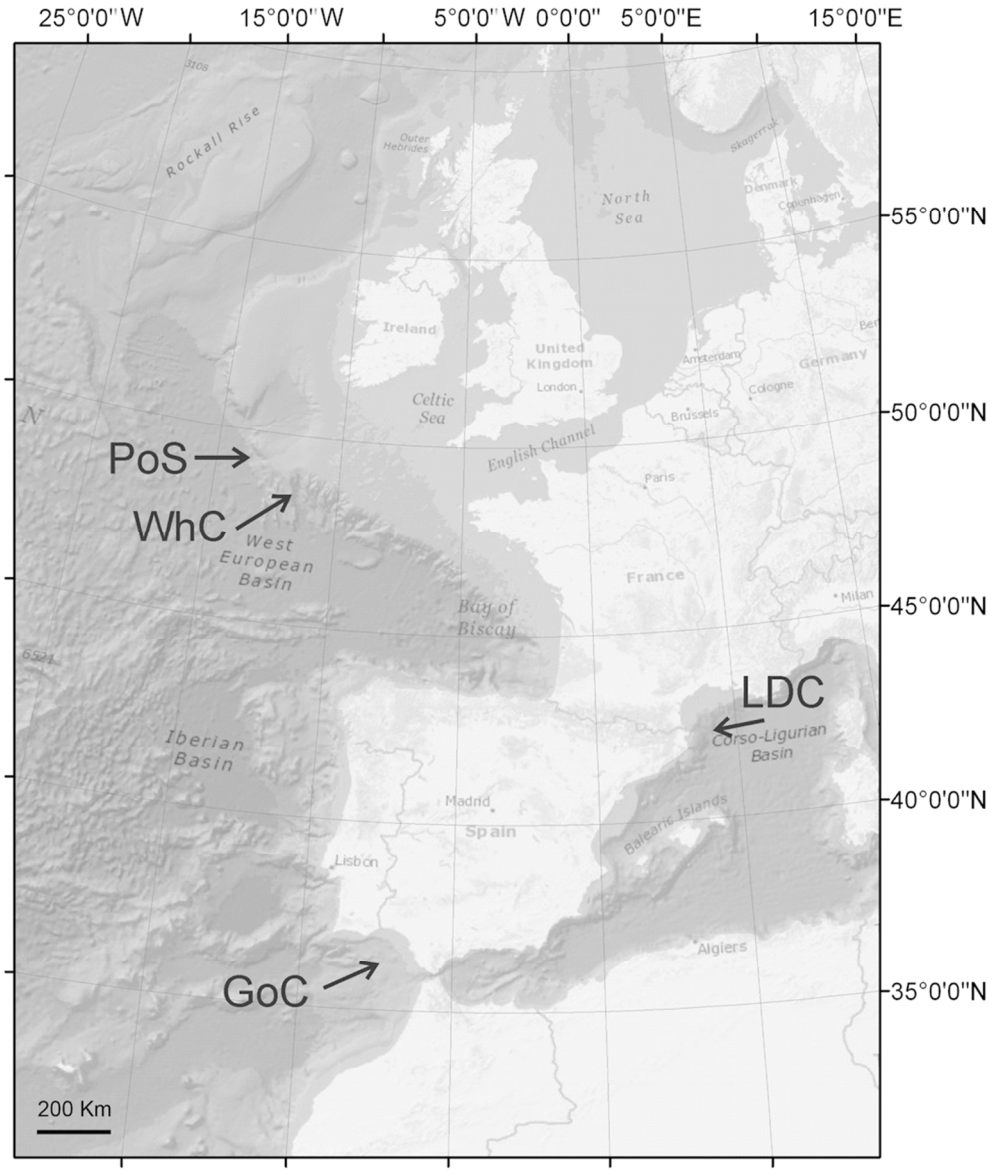

Figure 1: Map of sampling locations. PoS: Porcupine Seabight. WhC: Whittard Canyon. GoC: Gulf of Cadiz. LDC: Lacaze-Duthiers Canyon.
90x105mm (300 x 300 DPI)

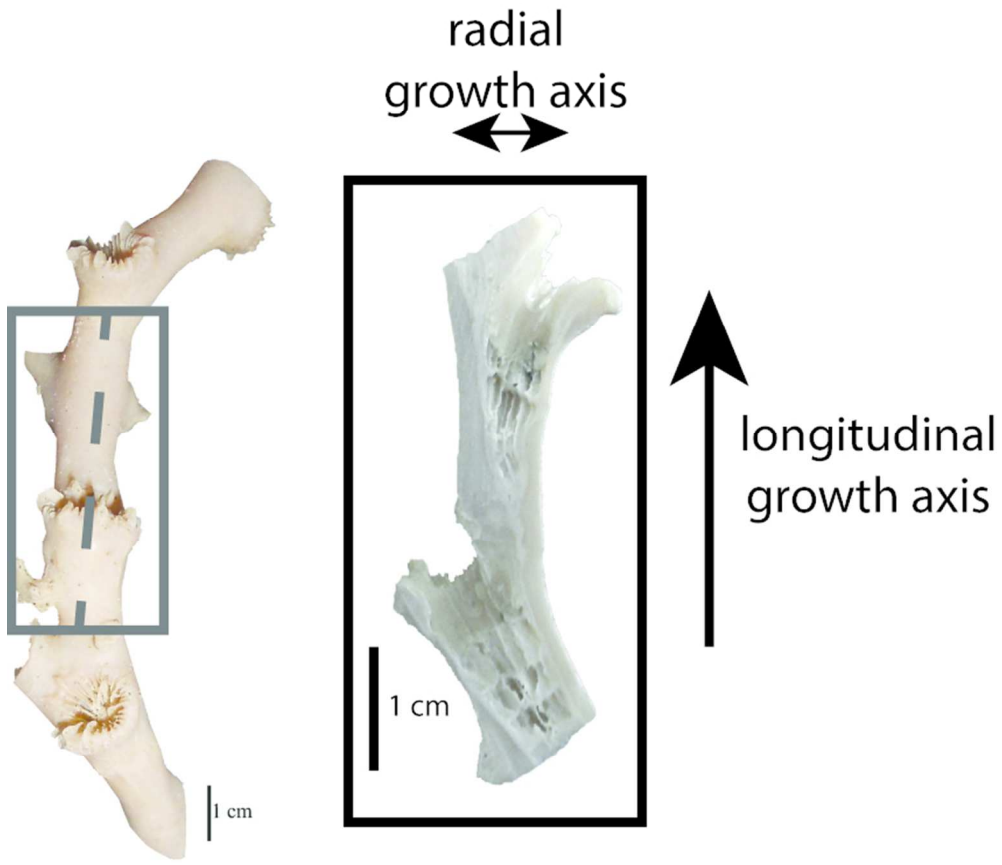

Figure 2: WhC-1 Lophelia pertusa specimen. Orientation of cutting is marked with a dashed line.
72x62mm (300 x 300 DPI)

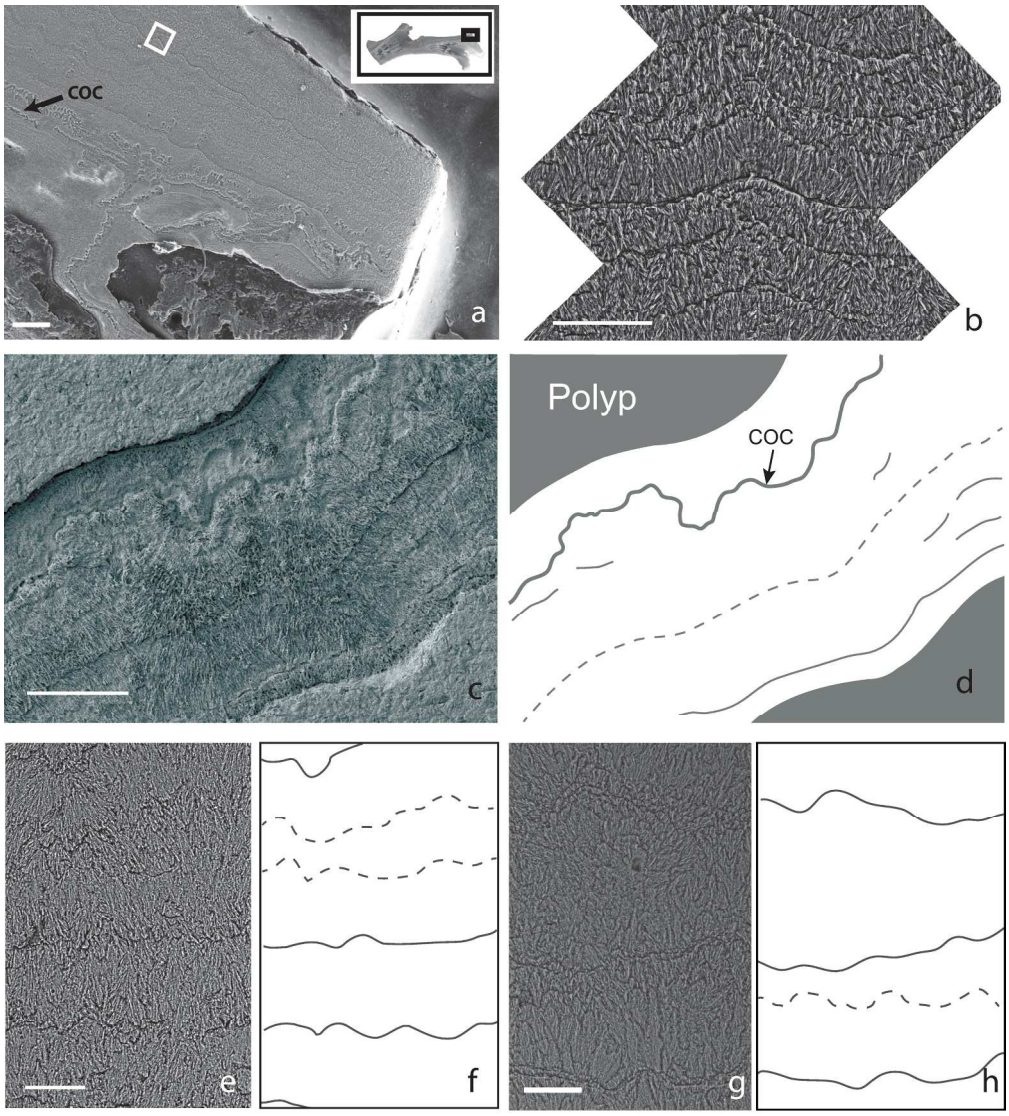

Figure 3: Micro-layers imaged in the theca wall of L. pertusa. a: In specimen WhC-1. The longitudinal growth direction is towards the bottom right and radial growth towards the upper right. The scale bar is 200 µm. b: Detail of the micro-layers on the area delimited by the white square in Figure 3a. Longitudinal growth direction is towards right. Radial growth direction is upward. Scale bar is 100 µm. c: Specimen LDC-5. The longitudinal growth direction is towards the upper right and radial growth towards the bottom right. The scale bar is 100 µm. d: Interpretation of c. e: Specimen GoC-2. The longitudinal growth direction is towards the right and radial growth towards the bottom. The scale bar is 50 µm. f: Interpretation of e. g: Specimen PoS-1. The longitudinal growth direction is towards the left and radial growth towards upward. The scale bar is 50 µm. h: Interpretation of g. COC: centres of calcification.
229x256mm (300 x 300 DPI)

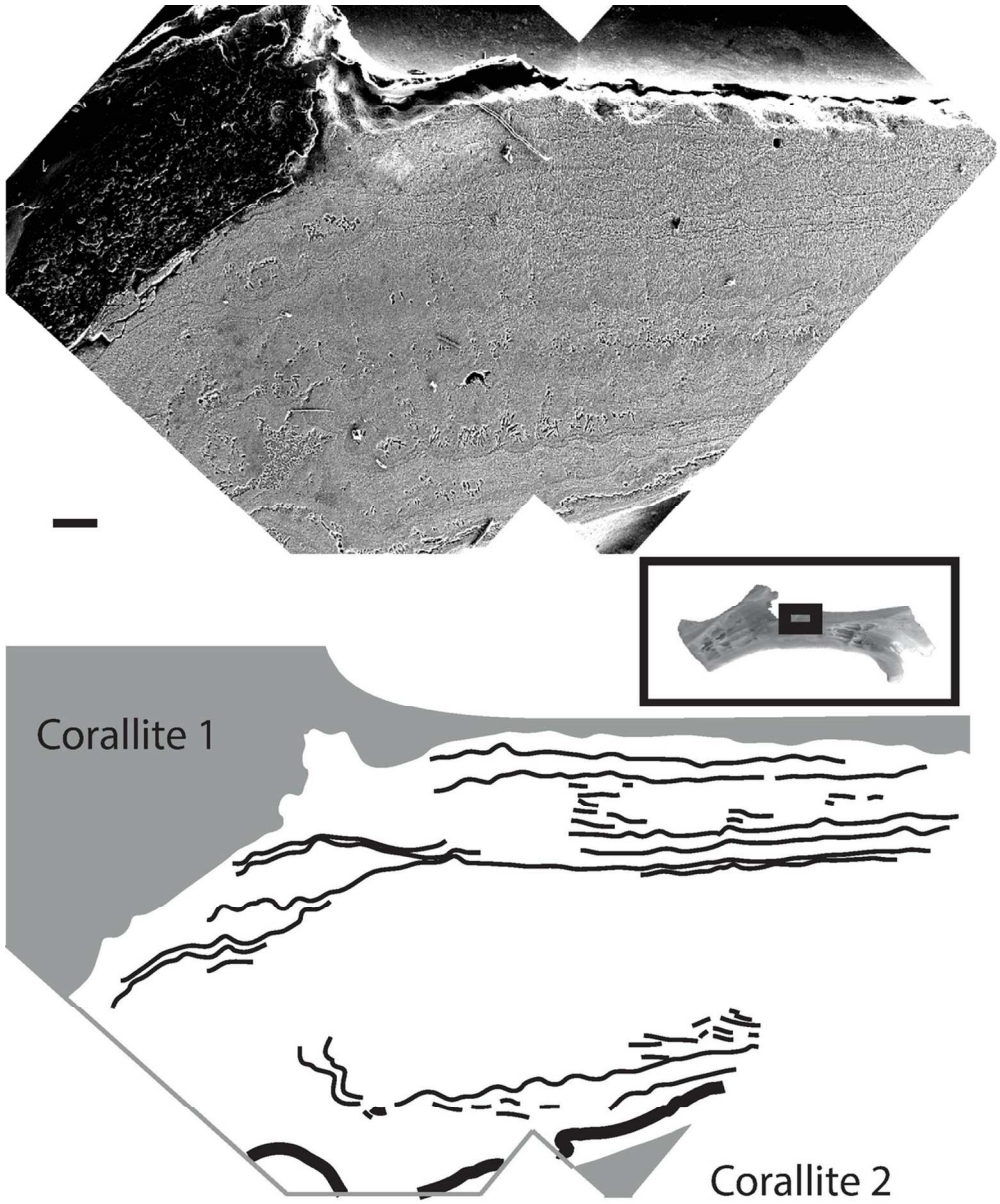

Figure 4: Absence of micro-layers in the middle of the wall near the corallite (on the left) in specimen WhC-1. Micro-layers are visible on the right hand side when moving away from the corallite (but are not visible in this view). The thick black curve highlights the COC. The scale bar is 200 μm long.
106x129mm (300 x 300 DPI)

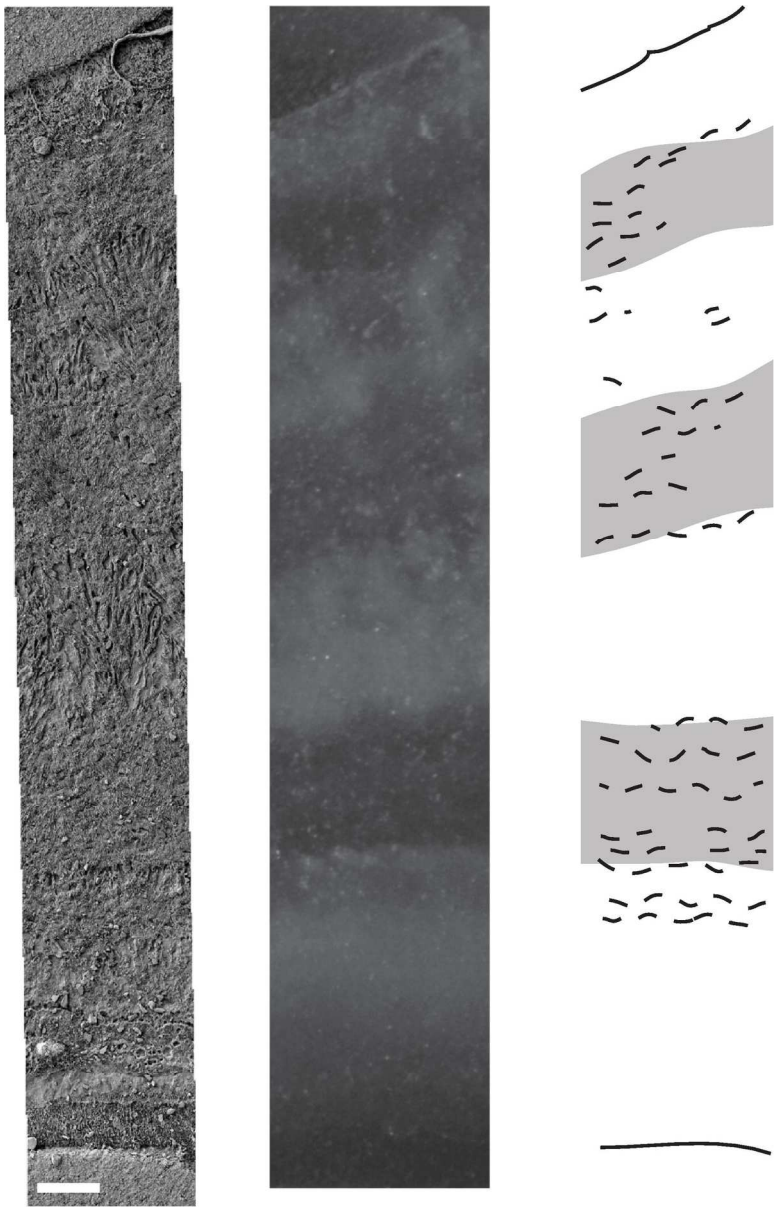

Figure 5: Opaque and translucent bands (centre) in relation to traces of micro-layers under SEM (left) in specimen WhC-3c and interpretation (right). On the right-hand side, white areas represent opaque bands and grey areas represent translucent bands, and black dashed lines represent micro-layers visible from the SEM figure. Longitudinal growth is towards the right; radial growth is towards the top. The scale bar is 100 µm long.
135x211mm (300 x 300 DPI)

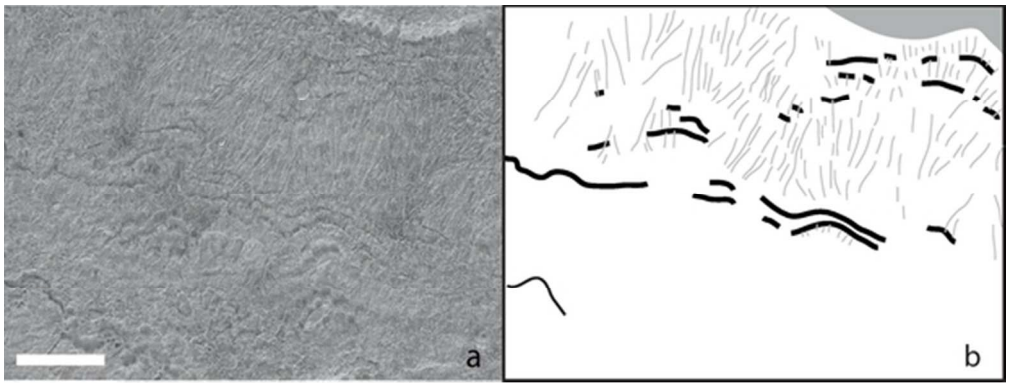

Figure 6: a: Micro-layers with no continuity visible in specimen GoC-2/2d. b: Interpretation of a. Black lines represent visible micro-layers and fine grey lines represent aragonite fibres. Note that micro-layers are visible only where aragonite fibres can be seen. Longitudinal growth direction is towards the right; radial growth direction is towards the top. The scale bar is 100 μm long.
52x19mm (300 x 300 DPI)

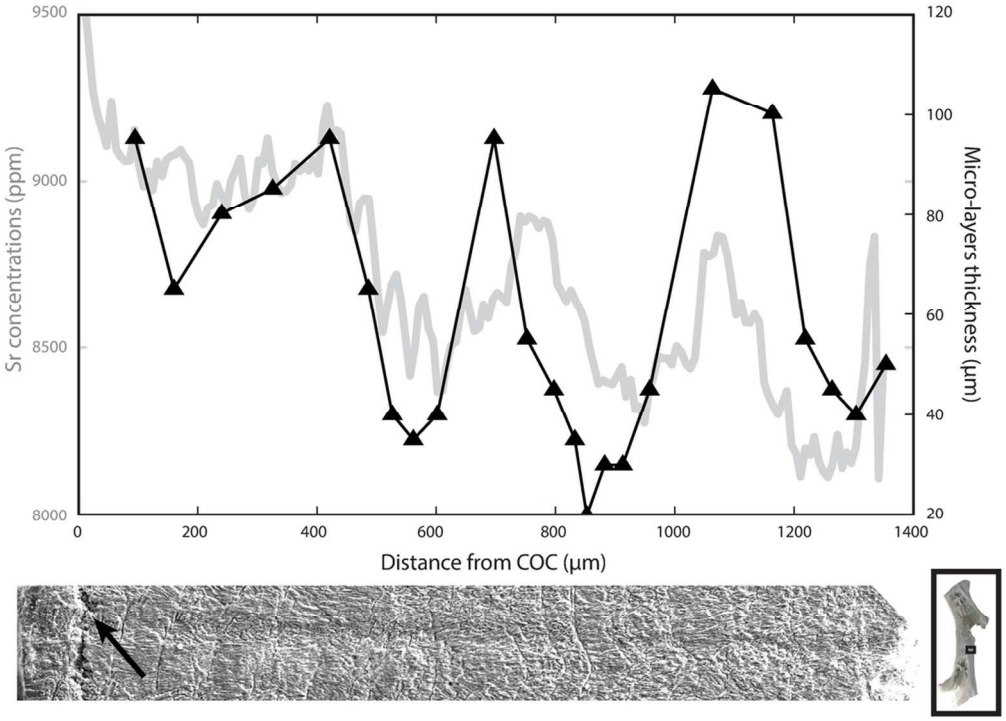

Figure 7: Strontium concentrations (in grey) across the wall of specimen WhC-1 in relation to micro-layer thickness (in black). The micro-layer thickness values are positioned at the center of each of these increments starting with the first complete (the space between the COC and the first increment was ignored). Sr concentrations have been smoothed using a moving average. Error bars for Sr concentrations are less than the line width. The arrow indicates the location of the COC.
100x71mm (300 x 300 DPI)

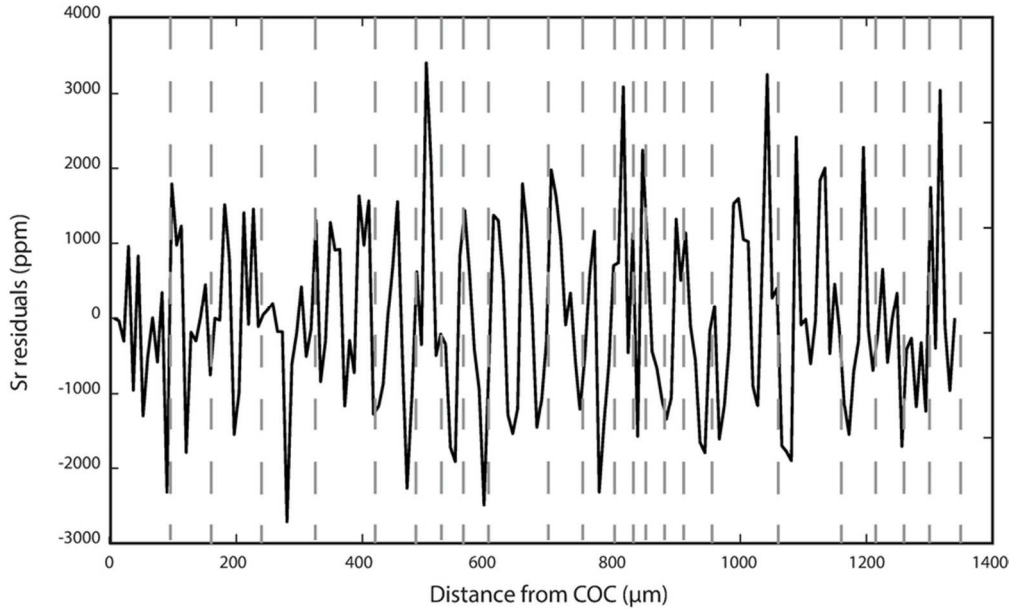

Figure 8: Residuals of strontium measurements on WhC-1 (in black) in relation to micro-layers occurrence (vertical grey dashed lines).
80x48mm (300 x 300 DPI)

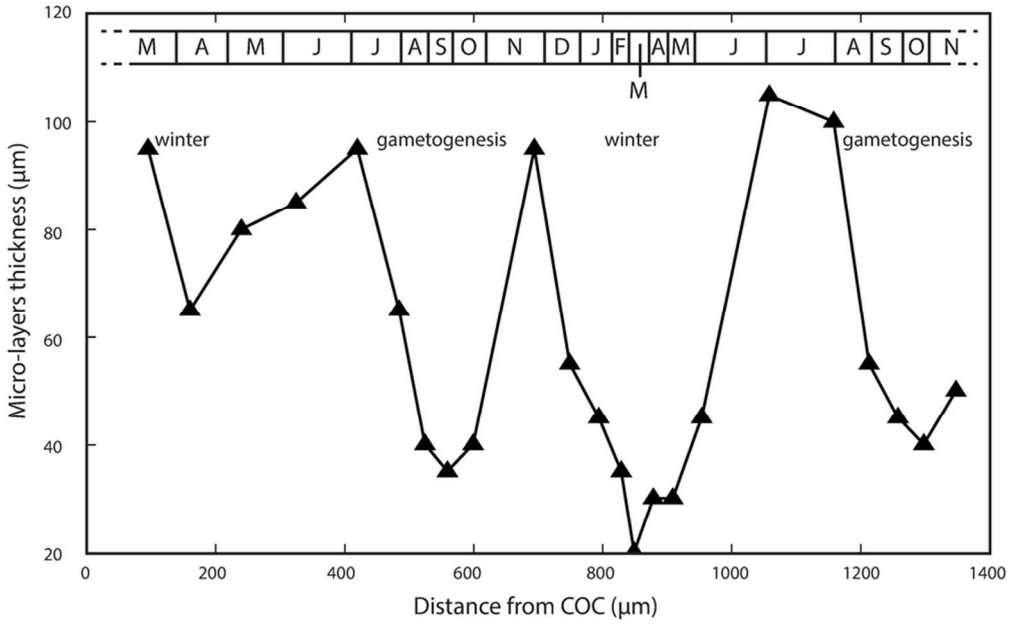

Figure 9: Micro-layers thickness and interpreted monthly calibration (on top) across the wall of WhC-1. The micro-layer starting at 1160 µm was used as the starting point of the proposed temporal frame. In this interpretation, 1 micro-layer is formed in 28 days.
84x51mm (300 x 300 DPI)